In-Flight Flow Visualization Using Infrared Imaging

J. M. Brandon,* G. S. Manuel,* R. E. Wright Jr.,† and B. J. Holmes‡
NASA Langley Research Center, Hampton, Virginia 23665

A flight-test investigation was conducted to evaluate infrared (IR) flow imaging techniques for boundary-layer flow visualization. The flight tests used a single-engine turboprop aircraft with a fiberglass-skinned natural laminar flow glove mounted on the left wing and an infrared imaging system to obtain flow visualization data. Data were compared to results obtained from other more conventional boundary-layer flow visualization methods and found to agree well. Test flights were conducted to determine the effect of test surface color on IR flow visualization results. In addition, flights were made during both night and daylight hours to assess the effect of solar radiation on the results. The investigation included an effort to visualize a vortex passing over the wing glove, but the tests provided only limited results.

Nomenclature

c = mean aerodynamic chord, ft
h_{c_l} = laminar flow average convection coefficient, Btu/h ft^2 °F
h_{c_t} = turbulent flow average convection coefficient, Btu/h ft^2 °F
H_p = pressure altitude, ft
k = thermal conductivity of air, Btu/h ft °F
K = recovery factor
l = characteristic length, ft
M = Mach number
P_r = Prandtl number
q_c = heat flux rate due to convection, Btu/ft^{2}h
q_r = heat flux rate due to radiation, Btu/ft^{2}h
q_s = heat flux rate due to solar radiation, Btu/ft^{2}h
R_e = Reynolds number
T_∞ = freestream temperature, °R
T_s = surface temperature, °R
V_i = indicated airspeed, kt
γ = specific heat ratio
ϵ = emittance
σ = Stefan-Boltzmann constant

Introduction

BOUNDARY-LAYER transition flow visualization is valuable for evaluation of laminar-flow airfoil performance. Popular techniques include sublimating chemicals,[1,2] liquid crystals,[3-5] and oil flow. Each of these methods has particular strengths and weaknesses. All require a coating of material appropriate to the test condition be applied to the surface being studied. Infrared (IR) flow visualization provides transition visualization without this requirement. This paper presents results of an evaluation of IR flow visualization in flight on a subsonic airplane with a natural laminar flow (NLF) glove as a test surface.

Researchers have presented results of previous studies using IR imaging for boundary-layer transition visualization in subsonic flows.[6-7] These two studies demonstrated that IR imaging could be effective in boundary-layer flow visualization; however, operational considerations for application of IR imaging have not previously been addressed. Specifically, these issues are mechanisms responsible for IR signatures, effect of sun position, feasibility of night testing, transient response characteristics, and the effect of test surface color.

Infrared boundary-layer transition visualization relies on the heat transfer properties of laminar and turbulent flow. In laminar flow, the heat transfer rate between the fluid and surface is low due to low rates of convection. Conversely, the turbulent boundary-layer flows exhibit higher rates of heat transfer due to increased rates of convection. This difference in heat transfer rate results in a surface temperature difference between laminar and turbulent areas. With proper emissivity of the test surface, these temperature differences can be observed using IR imaging equipment. In addition to transition visualization, IR imaging can locate the path of streamwise vortices passing near airframe surfaces. Streamwise vortices can be observed unaided, in flight, by natural condensation of moist air over the wing.[8] Research on the effects of these vortices on wing-flow characteristics can benefit from a flow visualization method, which can aid in vortex visualization. The path of a vortex over a wing surface should produce locally increased heat transfer due to the localized scrubbing action of the vorticity. The resulting temperature differential should be observable in the IR spectrum.

The IR flow visualization technique possesses several desirable characteristics: The technique is completely nonintrusive; it requires no surface coating, and it utilizes remote sensing. In addition, the same equipment is used for all flight conditions allowing testing at various flight conditions within the complete speed and/or altitude range of an airplane with one experimental setup. Such an arrangement reduces the flight hours required to obtain desired flow visualization results and thus reduces the cost of testing.

Flight Test Setup

Test Aircraft

A NASA T-34C, single-engine turboprop airplane with a NLF glove was used for this flight research (see Fig. 1). The airplane is unpressurized and has a two-place tandem cockpit arrangement. The experiments utilized the NLF glove on the left wing as the laminar flow test surface. The 92-in. chord, 3-ft span glove incorporates a NASA NLF(1)-0215F airfoil section.[9] This airfoil maintains a favorable pressure gradient from the leading edge to near 45% chord location on the upper surface at low angles of attack. Transition locations on the glove were previously documented in flight.[10] The glove

Received April 15, 1989; presented as Paper 88-2111 at the AIAA 4th Flight Test Conference, San Diego, CA, May 18-20, 1988; revision received Dec. 15, 1989.

*Research Engineer. Member AIAA.
†Research Engineer.
‡Head, Flight Applications Branch. Senior Member AIAA.

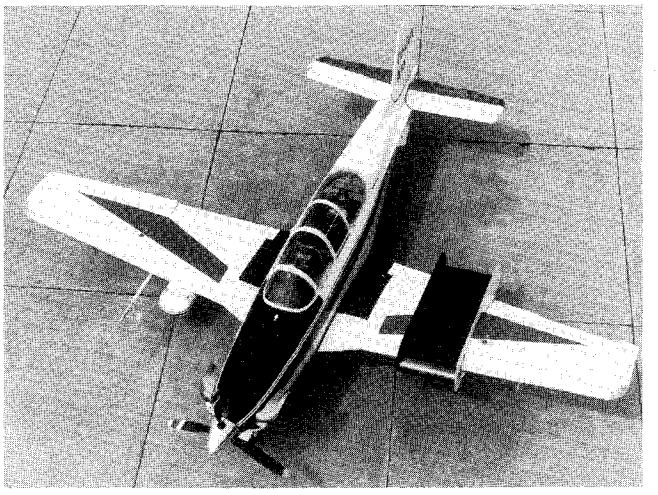

Fig. 1 Photograph of T-34C aircraft used in present study.

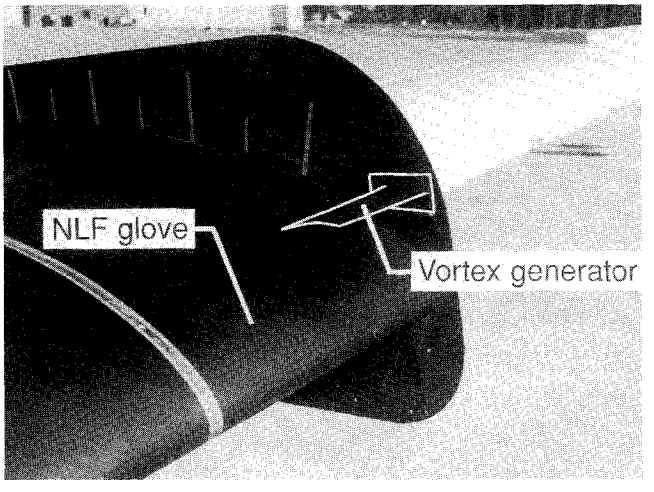

Fig. 2 Photograph of vortex generator installation on NLF glove.

skin is sheet aluminum covered with fiberglass. Aluminum endplates are attached to both inboard and outboard edges of the glove. Chordwise locations marked on the outboard endplate with aluminum tape aid in the analysis of flow visualization data. Flight tests were conducted with the NLF glove painted alternately black, white, and orange to assess the effect of color on the IR flow visualization results.

A vortex generator was mounted on the outboard fence during some of the test flights to attempt to visualize the vortex path as it passed over the wing. The vortex generator was an aluminum airfoil with an 8-in. span and 4-in. chord. Figure 2 shows a photograph of the vortex generator mounted on the glove.

Test Procedures and Conditions

Ground tests conducted with the engine running indicated that the hot engine exhaust passing between the glove and the IR imager created streaks in the IR image. In order to minimize this interference, flight-test procedures consisted of stabilizing on a steady-state condition and then reducing power to minimize the hot exhaust effect on the image. Indicated speed was held constant, and a steady shallow dive was allowed for the test points. Further ground tests were made to verify that IR energy from the engine exhaust pipe was not being reflected off of the NLF glove toward the IR camera.

Flight tests were conducted over a speed range from 80 to 210 kt indicated airspeed and a pressure altitude range of 3500–18,000 ft during daylight and night-time conditions. All data runs were conducted with the canopy open so that no loss of imager sensitivity occurred from IR absorption by the Plexiglas window.

Infrared Imager

An infrared imager with a nominal 2–5.5 μm spectral sensitivity range was used in the current tests. This model was selected based on the small size of the unit and its availability. The imager specifications are listed in Table 1. Figure 3 shows the camera and display unit. The camera is a mechanically scanned unit in which two orthogonally rotating prisms scan the image of the single-element, liquid-nitrogen-cooled, indium antimonide detector over the viewed scene. Camera sensitivity is controlled with apertures and optical filters positioned between the detector and the rotating prisms. The camera was fitted with a 33-mm focal length silicon lens, which provided a 20×20-deg^2 field of view. The sensitivity of the imager used in the current experiment is illustrated in Fig. 4.

The liquid nitrogen vapor pressure in the detector dewar was not controlled during these tests. Detector manufacturer's literature and unpublished test data generated at NASA-Langley indicate that the sensitivity of the unpressurized imager decreased with altitude, but no quantitative data have been obtained on the actual sensitivity loss. Operation of liquid-cooled detector imaging systems with standard display electronics in unpressurized aircraft at altitudes over 18,000 ft is not recommended due to sensitivity changes and possible arcing in the display unit.

The IR imager used in this test generates a nonstandard video format output, so a scan converter was used to generate video for recording on a conventional, portable videocassette recorder. The data presented in this report are photographs of a television monitor with the videocassette recorder operated in the still-frame mode. Step artifacts produced by the scan converter are evident in the photographs.

During the research flights, an experimenter in the rear seat of the aircraft adjusted the imager so that temperature gradients on the glove could be observed. The adjustments made included a range adjustment that controlled the overall sensitivity range in the picture. Typically the range was set at values of 2 or 5, which corresponded to a total temeprature range visible on the display unit of approximately 2 or 5°C, respectively. The other adjustment made was a black-level adjust-

Table 1 Imager specifications

Range of spectral sensitivity	1.3–5.5 μm
Temperature sensitivity	0.1°C at 30°C
Spatial resolution	3.4 μrad at 50% contrast
Time resolution	1/25 s (1 field)
Scan format	2500 lines/s, 6.25 frames/s, 4 fields/frame
Viewed field angle	20 × 20 deg
Scan converter resolution	8 bits, 100 samples/line

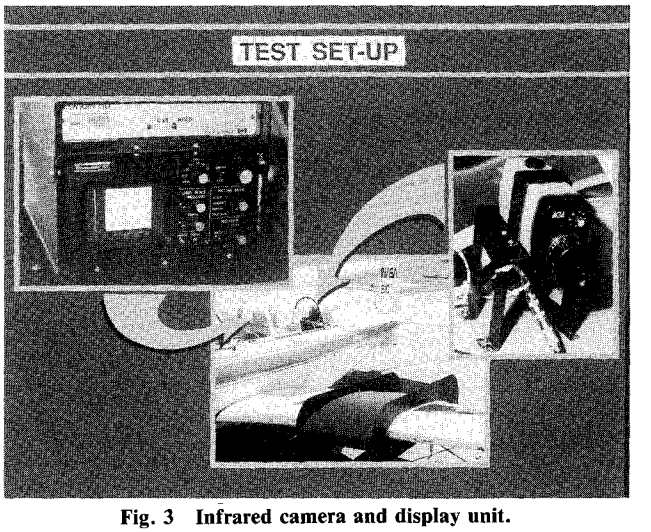

Fig. 3 Infrared camera and display unit.

ment, which set the temperature for a black image. This was adjusted to give the most contrast possible over the area of interest on the glove. All adjustments were made in flight while observing the image real-time on the display unit.

Thermodynamic Considerations

Before proceeding to the flight-data results, an overview of the physics involved in IR flow visualization provides background that is useful in the interpretation of data. Flow transition detection techniques can be classified according to the physical phenomena responded to, such as surface temperature, heat flux, shear stress or skin friction, or local flow-density gradients. An example of a shear stress technique is the use of liquid crystals, which during exposure to freestream airflow reflect different colors in response to local differences in laminar and and turbulent shear stresses. IR flow visualization, on the other hand, detects temperature differences between laminar and turbulent regions on a test surface.

An IR imager measures spatial distribution of energy in specific wavelength ranges radiated by a test surface. The spatial distributions of surface temperature and emittance provide image patterns in response to flow phenomena. The test surface temperature distribution has a mean, based on total heat balance factors and perturbations from the mean caused by local flow phenomena. The local perturbations result from two primary effects: compressibility heating and differences in convective heat-transfer coefficients as a function of local flow conditions (turbulent or laminar flow).

The average steady-state heat inputs to aircraft surfaces in flight during daylight hours include direct and reflected solar radiation; long-wave radiation emitted by the Earth, the atmosphere, and the aircraft engines and exhaust; convective heating by the boundary layer when its temperature is greater than the aircraft surface temperature; and radiation, conduction, and convection from aircraft components inside the structure. The daylight steady-state aircraft surface heat losses include long-wave radiation loss to space, the Earth, and any other material within the field of view of the aircraft surface; precipitation impingement and evaporation; and convective cooling if the surface temperature is higher than the boundary-layer temperature. During night-time hours, lack of solar radiation heating will result in aircraft surface temperatures much lower than during daylight hours.

Compressibility Heating

Temperature of the air at the surface of the wing is a function of Mach number and a temperature recovery factor K as shown in the following equation for ideal gas flow:

$$T_s = T_\infty \left\{1 + [(\gamma - 1)/2]\, KM^2\right\}$$

Normally, for adiabatic surfaces, $K = 0.84$ for laminar and $K = 0.86$–0.88 for turbulent boundary layers. Since the typical aircraft wing surfaces are not adiabatic, these values of K may be somewhat lower; however, the difference in turbulent and laminar recovery factors should remain relatively constant. As Mach number is increased, the recovery temperature at the wall through the turbulent boundary layer increases relative to the temperature through the laminar boundary layer. For a typical case, this difference would be expected to be on the order of 0.2–0.4°F at a Mach number of 0.3. At higher Mach numbers, the temperature differences due to the higher recovery factor for turbulent flow become more pronounced.

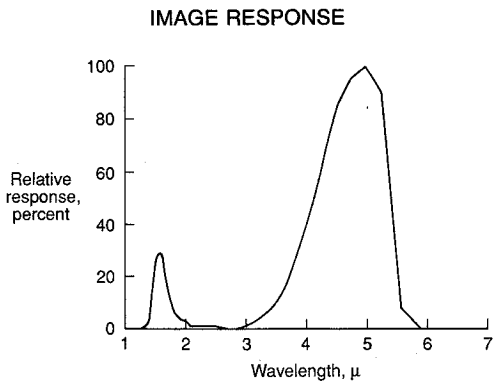

Fig. 4 Response of IR imager.

Convective Heat Transfer

At low subsonic speeds, a more powerful effect on the temperature at the wing is caused by convection. Because of increased shear stress and drag, the turbulent boundary layer exhibits a larger value of convection coefficient than the laminar boundary-layer flow. Heat flux due to convection is defined as

$$q_c = h_c\,(T_s - T_\infty)$$

For the laminar boundary layer, the average coefficient of convection can be approximated by

$$h_{c_L} = 0.664\,(k/1)\,R_{e1}^{1/2}\,P_r^{1/3}$$

The turbulent boundary layer average convection coefficient can similarly be approximated as

$$h_{c_T} = 0.036\,(k/1)\,R_{e1}^{0.8}\,P_r^{1/3}$$

To estimate a temperature difference between the laminar and turbulent flow areas, heat transfer due to radiation must also be considered. The wing surface constantly radiates heat energy to space at a rate described by the equation

$$q_r = \epsilon\sigma T_s^4$$

Assuming that the change in convection coefficients is the only factor differentiating the laminar and turbulent sections of the wing, from a heat transfer point of view, the preceding equations can be solved to provide surface temperature estimates using the following relationship for steady-state conditions:

$$q_s = q_c + q_r$$

This relationship and the following assumptions: $V_i = 180$ kt; $T_\infty = 59$°F; $\epsilon = 0.9$; $q_s = 412$ Btu/ft^{2}h; transition location = 40%c, predict a maximum temperature difference of 32°F between the laminar and turbulent flow regions.

Factors that affect transition detection using an IR imager include wing emittance in the imager passband, the imager spectral passband, the solar absorptance, the skin thermal lateral conductance and heat capacity, the data acquisition and processing techniques used, optical filtering, and intervening gas absorption and radiation. The emittance and solar absorption values were varied in these tests by painting the NLF glove. Three colors were tested—black, white, and orange. The emittance affects imager sensitivity directly since this parameter determines the amount of radiation available to be detected. Most nonmetallic pigment organic paints will have a moderately high emittance in the imager spectral passbands, typically 0.7 or greater. Polished aluminum, on the other hand, could have an emittance as low as 0.05. High target emittance will also help suppress spurious reflected radiation within the imager spectral passband. Emittance values of the three colors tested were between 0.8 and 0.9 in the imager passband. Actual surface emittance sensible by the IR imager is also a function of the angle between the imager and local surface target. Solar absorption affects imager sensitivity by elevating the temperature of the wing. The white painted wing had very little solar energy absorption, whereas the or-

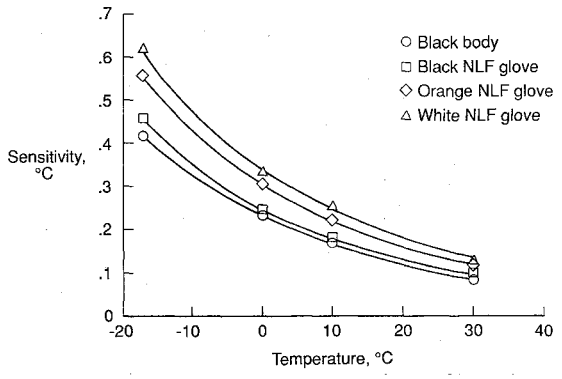

Fig. 5 Effect of target temperature on minimum detectable temperature gradient.

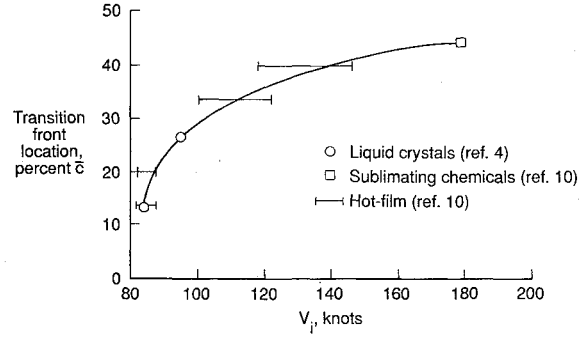

Fig. 6 Transition from location determined in previous studies.

ange and black painted surfaces absorbed progressively more solar energy resulting in higher temperature levels on the wing surface.

The sensitivity of the IR imager increases as the temperature of the target is increased. Figure 5 shows the relation of minimum detectable temperature with temperature level for the imager used in the current tests. High solar absorptance coatings on a low thermal conductance target and daytime testing helped keep the temperature level high and thus enhanced detection of transition from laminar to turbulent flow.

The low thermal conductivity of the fiberglass NLF glove helped reduce the conduction of heat between the laminar and turbulent portions of the wing allowing for nearly steady-state temperature differences to be maintained between the two flowfield areas on the wing. Additionally, the low thermal mass of the fiberglass allowed the temperature differences to occur rapidly for changing flight conditions.

Imager data acquisition techniques used in this experiment were photographic; the images, converted to standard video format, were played back and photographed in still-frame mode on the video monitor. Computerized image processing capability could be used to enhance the picture quality by performing background subtraction and image averaging for improved signal-to-noise ratio and to improve contrast (see Ref. 7).

Flight Test Results

Daylight – Black Glove

The primary configuration tested was the black NLF glove. This glove has been previously studied using sublimating chemical, liquid crystal, and hot film methods of flow transition detection.[4,10] The previously determined transition locations for a range of indicated speed is shown in Fig. 6. These data indicate a relatively wide transition zone between laminar and turbulent flow. In addition, the data indicate that the transition location remains relatively constant at airspeeds above 120 kt.

During the IR visualization flights, aircraft heading was maintained to reduce solar radiation in the form of glare reflecting into the IR camera. It was determined that the best results were obtained by flying headings that resulted in a sun position directly behind the IR camera. Failure to maintain the proper sun position relative to the NLF glove and IR camera resulted in reflections off of the glove that obscured the visualization of temperature differences on the wing caused by the varying flowfields of interest.

To build confidence in the IR flow visualization results initially, flights with sublimating chemicals were flown to compare directly with IR results. During these flights, a turbulent wedge was created by a piece of tape running down the center of the NLF glove. Figures 7 and 8 show a comparison of the IR visualization with sublimating chemical results at $V_i = 178$ knots and $H_p = 6500$ ft. The comparison indicates good agreement, with both techniques showing the transition wedge near the middle of the NLF glove and the transition front at about 43%c. The IR photograph shows that the laminar region is warmer (lighter color) than the turbulent region. This result is due to the increased convection coefficient of the turbulent boundary layer. The outside air temperature is lower than the NLF glove surface temperature due to solar heating, and the turbulent flow area is cooled at a faster rate than the laminar area.

Figures 9–12 show the movement of the transition location for indicated airspeeds of 187, 160, 120, and 100 kt, respectively. Figures 9 and 10 show transition at essentially the same location of about 43%c, as would be expected from previous data. As the aircraft speed is reduced, the transition front moves forward to about 34%c at $V_i = 120$ kt (see Fig. 11) and to about 20%c at $V_i = 100$ kt (see Fig. 12). Figure 13 shows a summary of the transition front locations determined by IR data across the speed range of the aircraft. Comparison with data from past studies shows good agreement with conventional flow visualization results at indicated airspeeds over 120 kt. At $V_i = 100$ kt, IR flow visualization showed the transition front at a more forward location than observed in the previous flow visualization results. This apparent difference in the transition location may be due to the relative position of the IR camera with respect to the NLF glove. At the forward locations on the glove, the angle between the imager and the surface of the glove is small, which may lead to difficulty in precisely locating the transition front location.

One primary focus of the current tests was to determine the important factors required for successful IR flow visualization of the boundary-layer flow. Tests were made to determine the time-dependent response of visible changes in the surface temperatures in response to changing flight conditions.

Two types of tests were performed to assess the effects of ambient temperature and to determine the transient characteristics of the IR images. Rapid ascents to cooler air were made, and the flow patterns on the wing were recorded upon reach-

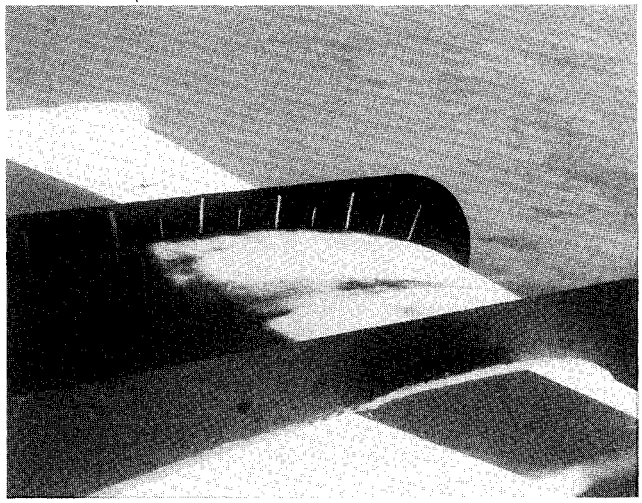

Fig. 7 Sublimating chemical pattern at $V_i = 178$ kt.

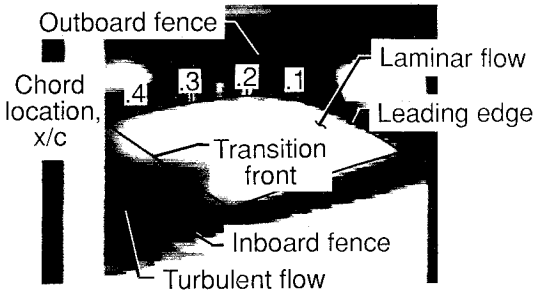

Fig. 8 Photograph of IR image at V_i = 178 kt.

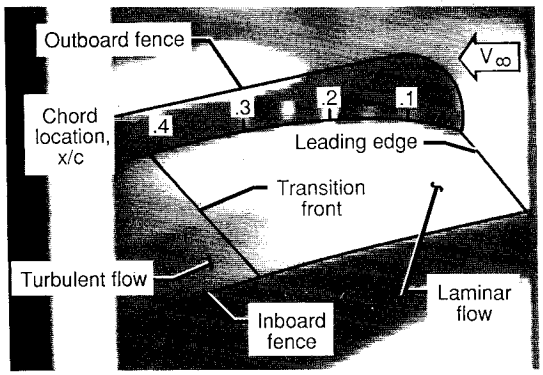

Fig. 9 Photograph of IR image at V_i = 187 kt.

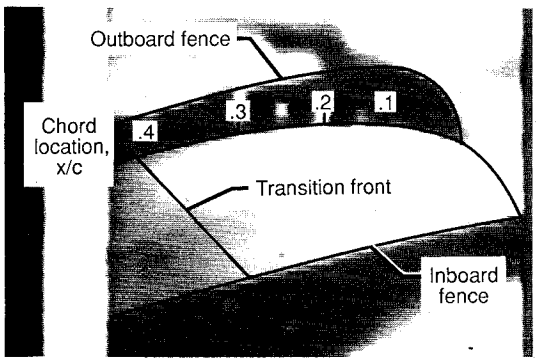

Fig. 10 Photograph of IR image at V_i = 160 kt.

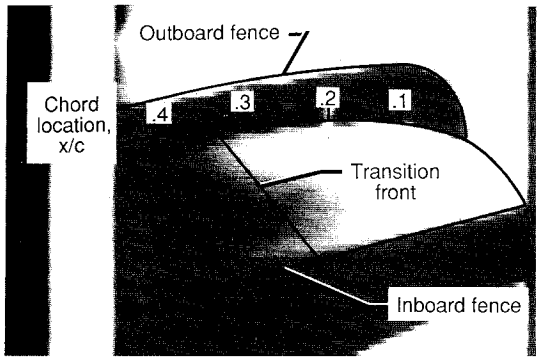

Fig. 11 Photograph of IR image at V_i = 120 kt.

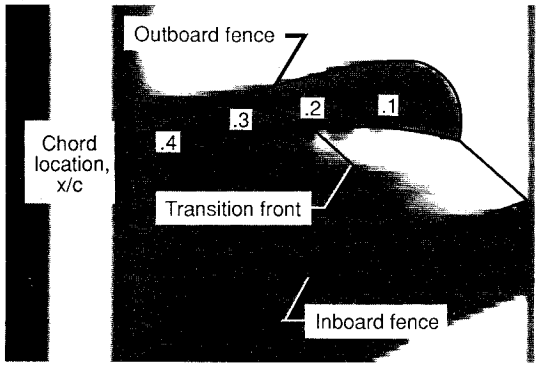

Fig. 12 Photograph of IR image at V_i = 100 kt.

ing altitude and then repeated after remaining at that temperature and altitude for several minutes. The other main test used to determine transient characteristics was a deceleration from high to low speed at a constant altitude. Data were recorded during the deceleration and then compared with images from steady-state conditions. Figures 14 and 15 show results at 140 kt immediately after reaching 10,000 ft altitude and then after 10 min, respectively. The climb was inititated from H_p = 3500 ft and was accomplished in approximately 3.5 min resulting in an outside temperature drop of 13°F. The initial image upon reaching H_p = 10,000 ft² (Fig. 14) shows a transition front location of about 38%c compared to about 41%c location shown in Fig. 15. Figure 16 shows results of a deceleration of 2 kt/s through 130 kt from an initial 180 kt. The image shows a streak where the transition front had been previously during the deceleration; however, a transition front can be seen at about 33%c, which compares favorably with the steady-state data of Figs. 10 and 11.

Night Results – Black Glove

During the daylight flights, it was very important to fly headings that prevented reflections of the sun off of the NLF glove toward the IR camera. At night, with no moon, the heading for the test flights was of little consequence in the data. At night, the factors in the heat balance equation change relative importance in that no solar radiation occurs and a greater amount of radiation from the NLF glove to space is present. These effects greatly reduce the surface temperature of the glove and, therefore, as just mentioned, decrease the

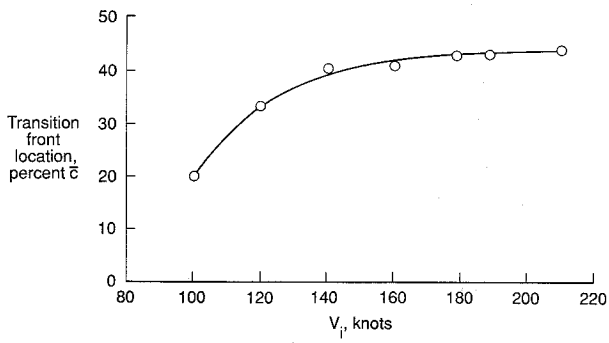

Fig. 13 Summary of IR transition front location results.

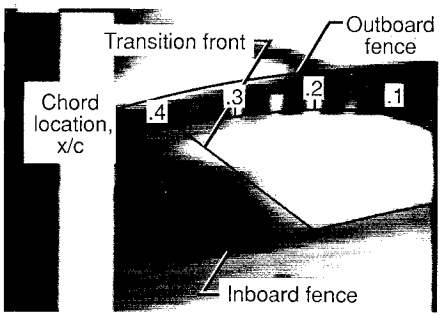

Fig. 14 Photograph of IR image initially; V_i = 140 kt.

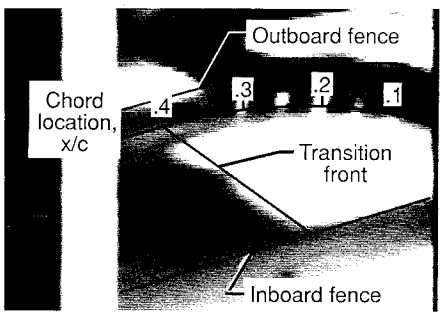

Fig. 15 Photograph of IR image after 10 min; V_i = 140 kt, H_p = 10,000 ft.

sensitivity of the imager and the probability of transition detection.

Because of the loss in sensitivity and the transient nature of the image, the steady-state level flight-test techniques used for the night-time tests were unsuccessful at low speeds. To utilize convection to provide heat differences on the wing in a quasi-steady manner, heat had to be added or removed from the NLF glove. To accomplish this, the aircraft was flown to a high altitude and allowed to cold soak. To begin the data run, a constant speed descent was initiated. This descent brought the aircraft into warmer air so that the convection tended to heat the wing as the aircraft descended. Using this technique, the color pattern on the IR images is reversed from that seen during the day flights. Figure 17 shows the laminar flow area as dark and the turbulent region as light. The flight condition for Fig. 17 was 210 kt, descending from 17,500 ft. Figure 18 shows another flight before sunrise at 190 kt level at 10,000 ft. Figure 18 shows a turbulent wedge caused by a particle on the forward upper surface of the wing. At the higher speeds, such as in Figs. 17 and 18, steady-state conditions on the wing were obtained at constant altitude. This may have been due to the Mach heating effect just mentioned. The recovery temperature through the turbulent boundary layer is greater than that through a laminar boundary layer resulting in the kind of image seen at night. Therefore, high speed and descent through warmer air combine to produce the best flow visualization images during night-time hours.

Effect of Surface Color

To assess the effect of surface color on the usefulness of IR imaging for flow visualization, tests were conducted with the NLF glove painted white and then orange in addition to black. These colors were chosen based on their absorptance and emittance characteristics. White has a very low absorptance to the solar radiation and a low IR emittance. Orange is approximately in between the white and black colors in these qualities.

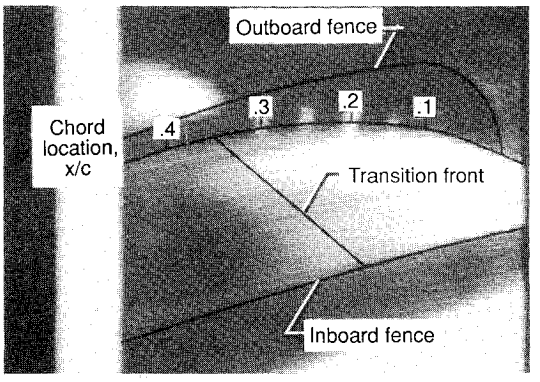

Fig. 16 Deceleration at V_i = 130 knots from V_i = 180 kt, 2 kt/s.

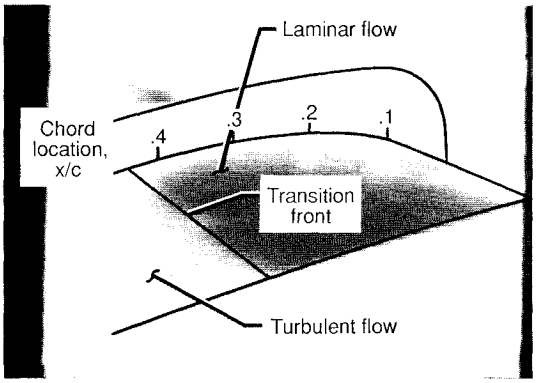

Fig. 17 Night IR image at V_i = 210 kt.

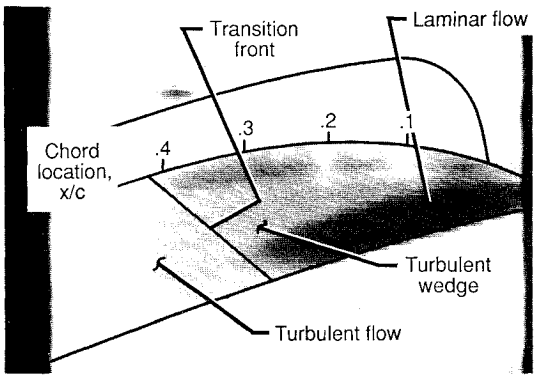

Fig. 18 Night IR image with turbulent wedge; V_i = 180 kt.

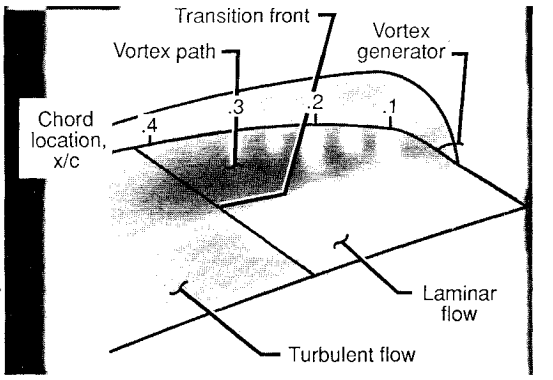

Fig. 19 IR image of NLF glove with vortex generator, V_i = 210 kt.

The white glove was flown during daylight hours and at night. Results of the daylight flights indicated that the white reflected the solar radiation at too great an extent for the imager to be able to identify the very small temperature gradients on the glove due to flow differences. At night, with a full moon, the results were very much the same as during the day. The reflected moon radiation obscured the temperature differences on the wing. The white NLF glove was also flown on a moonless night. Here, results were similar to that seen with the black NLF glove, however, the contrast in the picture with the white glove was reduced.

The orange glove was flown during the day only. Results for this color on the NLF glove were very similar to that seen for the white glove during the day. No flow visualization results were seen due to the reflection of the solar radiation.

Vortex Imaging Experiment

In addition to laminar and turbulent flow boundaries on a wing, other flowfield characteristics need to be observed for effective evaluation and understanding of a particular configuration. One flow of particular interest is vortex flow passing over the wing surface. The temperature in the vortex core is reduced from the freestream flow temperature due to low pressure (isentropic expansion) and high velocity in the vortex core. In addition, as the vortex passes over the wing surface, the "scrubbing" action of the vortex flow will increase the rate of heat convection in that area.

Figure 19 shows the results of a test flight with a vortex generator mounted near the leading edge of the NLF glove. The photograph represents the conditions at 210 kt at 17,500 ft altitude. At this condition, a clearly visible vortex was observed due to condensation of moisture in the air. The IR picture shows a cool area on the outboard area of the glove below the vortex. The laminar flow is apparently lost under the vortex. The inboard side shows the normal region of laminar flow. Although the IR image did not show a discrete vortex, it did identify a region of influence on the glove of the vortex.

Concluding Remarks

A flight-test investigation was conducted to evaluate IR flow visualization techniques for boundary-layer flow visualization. The flight tests used a single-engine turboprop aircraft with a fiberglass-skinned natural laminar flow glove mounted on the left wing. The flight tests were conducted using an IR imaging system to obtain flow visualization data. Results of the investigation can be summarized as follows:

1) Flow visualization using IR imaging was found to be a practical and useful tool in the analysis of flow conditions over a wing segment. The transition front from laminar to turbulent flow was readily identified for a variety of flight conditions. Turbulent transition wedges were also easily seen. Flowfield observations correlated well with results from previous studies.

2) Important characteristics for successful IR flow visualization include a skin surface with a low coefficient of conduction to allow a long-term temperature difference between flowfield areas rather than highly transient conditions and a surface color that emits sufficient energy in the imager sensitivity passband. Daylight provided energy to give a steady-state heat flux condition on the wing surface allowing for effective flow visualization. Night flights gave good results but required higher speeds or altitude change to produce a steady temperature difference between the two flowfield areas on the wing.

3) Direct visualization of a vortex traveling over the wing was unsuccessful using the IR imager; however, a region of influence of the vortex on the NLF glove was observed.

References

[1]Pringle, G. E., and Main-Smith, J. D., "Boundary-Layer Transition Indicated by Sublimation," Royal Aircraft Establishment, Farnborough, Hampshire, England, TN No. Aero. 1952, June 1945.

[2]Obara, C.J., "Boundary-Layer Flow Visualization for Flight Testing. Natural Laminar Flow Aircraft Certification Workshop," NASA CP-2413, May 1986.

[3]Holmes, B. J., Gall, P. D., Croom, C. C., Manuel, G. S., and Kelliher, W. C., "A New Method for Laminar Boundary Layer Transition Visualization in Flight—Color Changes in Liquid Crystal Coatings," NASA TM-87666, Jan. 1986.

[4]Gall, P.D., and Holmes, B.J., "Liquid Crystals for High Altitude In-Flight Boundary Layer Flow Visualization," AIAA Paper 86-2592, Sept. 1986.

[5]Holmes, B.J., and Obara, C.J., "Advances in Flow Visualization Using Liquid Crystal Coatings." Society of Automotive Engineers, Warrendale, PA, Paper 871017, 1987.

[6]Quast, A., "Detection of Transition by Infrared Image Technique" *Proceedings of the International Congress on Instrumentation in Aerospace Simulation Facilities*, IEEE, New York, June 1987.

[7]Bouchardy, A.M., Durand, G., and Gauffre, G., "Processing of Infrared Thermal Images for Aerodynamic Research." ONERA TP-1983-32, April 1983.

[8]Campbell, J. F., Chambers, J. R., and Rumsey, C. L., "Observation of Airplane Flow Fields by Natural Condensation Effects," AIAA Paper 88-0191, Jan. 1988.

[9]Somers, D. M., "Design and Experimental Results for a Flapped Natural Laminar Flow Airfoil for General Aviation Applications," NASA TP-1865, June 1981.

[10]Obara, C.J., and Holmes, B.J., "Flight Measured Laminar Boundary-Layer Transition Phenomena Including Stability Theory Analysis," NASA TP-2417, April 1985.